HEPATOLOGY

HEPATOLOGY, VOL. 69, NO. 1, 2019

Dual-Specificity Phosphatase 9 Protects Against Nonalcoholic Fatty Liver Disease in Mice Through ASK1 Suppression

Ping Ye,[1*] Mei Xiang,[1*] Hua Liao,[1*] Jijun Liu,[1] Hongbo Luo,[1] Yayun Wang,[1] Ling Huang,[1] Manhua Chen,[1] and Jiahong Xia[2]

Nonalcoholic fatty liver disease (NAFLD), ranging from nonalcoholic fatty liver to nonalcoholic steatohepatitis (NASH), is the leading cause of chronic liver diseases. Until now, no medications for NAFLD have been approved by relevant governmental agencies. Dual-specificity phosphatase 9 (Dusp9) is a member of the DUSP protein family. Dusp9 is expressed in insulin-sensitive tissues, and its expression may be modified with the development of insulin resistance (IR). However, the molecular targets and mechanisms of Dusp9 action on NAFLD and NASH remain poorly understood. In this study, using conditional liver-specific Dusp9-knockout (Dusp9-CKO) mice and Dusp9-transgenic mice, we showed that Dusp9 was a key suppressor of high-fat diet–induced hepatic steatosis and inflammatory responses and that Dusp9 deficiency aggravated high-fat high-cholesterol diet–induced liver fibrosis. Dusp9 was shown to exert its effects by blocking apoptosis signal–regulating kinase 1 (ASK1) phosphorylation and the subsequent activation of p38 and c-Jun NH2-terminal kinase signaling. *Conclusion:* Hepatocyte Dusp9 prevents NAFLD and NASH progression in mice, including lipid accumulation, glucose metabolism disorders, and enhanced inflammation and liver fibrosis, in an ASK1-dependent manner; these findings suggest that Dusp9 may be a promising therapeutic target for the treatment of NAFLD and NASH. (Hepatology 2019;69:76-93).

Nonalcoholic fatty liver disease (NAFLD), characterized by lipid accumulation in the liver, poses a great threat to general health, especially at younger ages; and nonalcoholic steatohepatitis (NASH), characterized by chronic inflammation in combination with type 2 diabetes and obesity, represents the most extreme form of NAFLD and is considered a major cause of hepatic

Abbreviations: AdGFP, adenoviral green fluorescent protein; ALP, alkaline phosphatase; ALT, alanine aminotransferase; ANOVA, analysis of variance; ASK1, apoptosis signal–regulating kinase 1; AST, aspartate aminotransferase; AUC, area under the curve; CD, cluster of differentiation; cDNA, complementary DNA; CKO, conditional knockout; Dusp9, dual-specificity phosphatase 9; ERK, extracellular signal–regulated kinase; FBG, fasting blood glucose; FINS, fasting serum insulin; GAPDH, glyceraldehyde 3-phosphate dehydrogenase; G6PC, glucose-6-phosphatase catalytic subunit; GSK3β, glycogen synthase kinase 3 beta; GST, glutathione S-transferase; GTT, glucose tolerance test; HA, hemagglutinin; H&E, hematoxylin and eosin; HFD, high-fat diet; HFHC, high-fat high-cholesterol diet; HOMA-IR, homeostasis model assessment of insulin resistance; IKK-β, inhibitor of nuclear factor kappa B kinase subunit beta; IP, immunoprecipitation; IR, insulin resistance; IRS1, insulin receptor substrate 1; ITT, insulin tolerance test; JNK, c-Jun NH2- terminal kinase; LW/BW, liver-to-body weight; MAPK, mitogen-activated protein kinase; MKK4/7, MAPK kinase 4/7; NAFLD, nonalcoholic fatty liver disease; NAS, NAFLD activity score; NASH, nonalcoholic steatohepatitis; NCD, normal control chow diet; NEFA, nonesterified fatty acid; NF-κB, nuclear factor kappa B; OA, oleic acid; PA, palmitate; PCK1, phosphoenolpyruvate carboxykinase 1; PPARα, peroxisome proliferator–activated receptor alpha; TC, total cholesterol; TG, transgenic; TNF, tumor necrosis factor; WT, wild type.

Received April 24, 2018; accepted June 26, 2018.

Additional Supporting Information may be found at onlinelibrary.wiley.com/doi/10.1002/hep.30198/suppinfo.

**These authors contributed equally to this work.*

Supported by grants from the National Natural Science Foundation of China (81730015, 81470482, and 81600186).

View this article online at wileyonlinelibrary.com.

DOI 10.1002/hep.30198

Potential conflict of interest: Nothing to report.

cirrhosis of unknown etiology.[1] It is estimated that approximately 20% of people with NAFLD have NASH, which in the United States affects approximately 3%-12% of adults.[2] The increasing incidence of NASH suggests that it may be the leading cause of liver failure in the next decade. Nonetheless, the underlying mechanisms of NAFLD and NASH remain unclear. To date, no effective medications are available for the treatment of NAFLD and NASH. Some researchers believe that selectively modulating key signaling pathways may be a feasible approach for the treatment of NAFLD.

Dual-specificity phosphatase 9 (Dusp9) is a member of the DUSP protein family, which dephosphorylates the threonine/serine and tyrosine residues of their substrates.[3] Dusp9 has been shown to be expressed in insulin-sensitive tissues, and its expression may undergo changes when insulin resistance (IR) develops.[4] In our preliminary experiments, we observed that Dusp9 expression was remarkably decreased in the liver tissue of mice fed a high-fat diet (HFD), eventually leading to NAFLD. However, the molecular targets and mechanism of Dusp9 action in NAFLD and NASH are still poorly understood. Dusp9 contains a cluster of basic amino acids known as the mitogen-activated protein kinase (MAPK)–binding motif or kinase-interacting motif, which down-regulates MAPK pathways involved in a wide array of cellular responses, including cell differentiation, proliferation, cell cycle regulation, and apoptosis.[5,6] Dusp9 has a substrate preference for extracellular signal–related kinases 1/2 (ERK1/2), c-Jun NH2-terminal kinase (JNK), and p38,[3,7,8] which are all implicated in the development of NAFLD and NASH.[9]

In view of the aforementioned findings, we hypothesized that Dusp9 may participate in lipid accumulation in hepatocytes and inflammatory responses in the progression of NAFLD and NASH. In fact, heterologous expression of Dusp9 in preadipocytes significantly blocked insulin-induced adipogenesis, and Dusp9 overexpression in adipocytes inhibited insulin-stimulated glucose uptake.[10] Nevertheless, the specific roles of Dusp9 in hepatocytes and the mechanisms by which Dusp9 mediates these obesity-related metabolic complications remain elusive. In this study, using conditional liver-specific Dusp9-knockout (Dusp9-CKO) mice and Dusp9-transgenic (Dusp9-TG) mice, we examined the effects of Dusp9 on obesity-associated pathological conditions, specifically focusing on the regulatory effects of Dusp9 on NAFLD and NASH.

Materials and Methods

ANIMAL MODELS

Adult male mice (C57BL/6), 8-10 weeks old (weighing 19-30 g), were housed at 23 ± 2°C under a 12-hour light/dark cycle with free access to water and food. The mice were fed an HFD (60.9% fat, 21.8% carbohydrate, and 18.3% protein; D12492; Research Diets) for various periods of time (2-24 weeks), a high-fat high-cholesterol diet (HFHC) (42% fat, 44% carbohydrate, 14% protein, and 0.2% cholesterol; TP26304; Trophic Diets, Nantong, China) for 16 weeks, or a normal control chow diet (NCD) (4% fat, 78% carbohydrate, and 18% protein; D12450J; Research Diets). Eight-week-old male genetically

ARTICLE INFORMATION:

From the [1]Department of Cardiology, The Central Hospital of Wuhan; [2]Department of Cardiovascular Surgery, Union Hospital, Tongji Medical College, Huazhong University of Science and Technology, Wuhan, China.

ADDRESS CORRESPONDENCE AND REPRINT REQUESTS TO:

Jiahong Xia, M.D., Ph.D.
Department of Cardiovascular Surgery, Union Hospital
Tongji Medical College, Huazhong University of Science and Technology
No. 1277, Jiefang Road
Wuhan 430022, China
E-mail: jiahong.xia@hust.edu.cn
or

Manhua Chen, M.D.
Department of Cardiology, Central Hospital of Wuhan
Tongji Medical College, Huazhong University of Science and Technology
No. 26 Shengli Street
Wuhan 430014, China
E-mail: cmh_centre@163.com

obese mice (*ob/ob*, B6/JNju-Lep^{em1Cd25}/Nju, N000103; Nanjing Biomedical Research Institute of Nanjing University) were fed the NCD and served as another fatty liver model.

ISOLATION AND CULTURE OF PRIMARY HEPATOCYTES

Primary hepatocytes were isolated from mice 6-8 weeks old. First, the animals were anesthetized by pentobarbital sodium. Then, the abdominal cavity was opened, and the liver portal vein was perfused with 45 mL of liver perfusion medium *in situ* to remove the blood. Perfusion with liver digestion medium was then performed for 5 minutes at a rate of 2 mL/minute. Subsequently, the liver was excised, minced, and filtered through a steel mesh. Primary hepatocytes were separated by centrifugation at 50*g* for 5 minutes and then purified in 50% Percoll solution. The purified hepatocytes were cultured in Dulbecco's modified Eagle's medium (DMEM) supplemented with 10% fetal bovine serum and 1% penicillin-streptomycin in a 5% carbon dioxide/water–saturated incubator at 37°C. To establish an *in vitro* model of hepatic steatosis in hepatocytes, palmitate (PA; 0.3 mM) was added to the medium, and the hepatocytes were incubated for an additional 24 hours.

WESTERN BLOTTING

Total protein was isolated from tissues or cells in radio immunoprecipitation assay lysis buffer, and protein concentrations were determined using the Pierce BCA Protein Assay Kit. Protein was loaded (40-50 μg) on a 10% sodium dodecyl sulfate–polyacrylamide gel electrophoresis (SDS-PAGE) gel, transferred to a polyvinylidene difluoride membrane, and incubated with corresponding primary antibodies overnight at 4°C. After incubation with peroxidase-conjugated secondary antibodies (Jackson Immunoresearch Laboratories, West Grove, PA; 1:10,000 dilution), bands were visualized with the ChemiDoc XRS+ imaging system (Bio-Rad, Hercules, CA). Protein expression was quantified with Image Lab Software and normalized to the housekeeping gene glyceraldehyde 3-phosphate dehydrogenase (GAPDH). Antibodies are listed in Supporting Table S1.

IMMUNOHISTOCHEMICAL ANALYSIS

For immunohistochemistry, paraffin-embedded sections were labeled with primary antibodies overnight and incubated with horseradish peroxidase–conjugated secondary antibodies. Immunohistochemical staining was visualized using 3,3′-diaminobenzidine (no. ZLI-9032; Zhongshan Biotech, Beijing, China). A Dusp9 monoclonal antibody (10826-1-AP, 1:200; Proteintech) was used as the primary antibody to visualize the expression of Dusp9 in hepatocytes. Images were acquired by a light microscope (Olympus, Tokyo, Japan).

MICE

Hepatocyte-specific Dusp9-deficient mice (Dusp9-CKO) were obtained using clustered regularly interspaced short palindromic repeats (CRISPR)/CRISPR-associated 9 methods. The third and fourth exons were flanked by loxP sites, and two single-guide RNAs (sgRNA1 and sgRNA2) targeting intron 2 and the noncoding region of exon 4 were designed. The donor vector containing exon 3 and the coding region of exon 4 was flanked by two loxP sites. PCR primers P1 to P5 were used for identification and are listed in Supporting Table S2. All products were confirmed by sequencing. Dusp9-CKO mice were generated by mating Dusp9-flox mice with albumin–cyclization recombination (Cre) mice (Jackson Laboratory, Bar Harbor, ME). Dusp9-flox (flox) littermates were used as controls for Dusp9-CKO (CKO) mice.

Full-length Dusp9 complementary DNA (cDNA) was inserted after CAG-loxp-CAT-loxp cassettes and microinjected into fertilized embryos (C57BL/6J background). Successful insertion was confirmed by genotyping using PCR and tail genomic DNA with the primers 5-CATGTTGGATCGATCCCCG-3 and 5-CATCCCACTCTTCTTTGGCC-3. Founder mice were crossed with albumin-Cre mice to obtain hepatocyte-specific Dusp9-TG mice. The CAG-loxp-CAT-loxp-Dusp9 mice (control mice) were used as controls.

HISTOLOGICAL ANALYSIS

Liver sections were paraffin-embedded and hematoxylin-eosin (H&E)–stained to visualize the pattern

of lipid accumulation. Oil red O staining of frozen liver sections was used to assess lipid droplet accumulation. Images were acquired by a light microscope (Olympus). Liver fibrosis was assessed by picrosirius red (26357-02; Hede Biotechnology Co., Ltd.) staining. Fibrotic areas were measured using a digital image analysis system (Image-Pro Plus, version 6.0).

The NAFLD activity score (NAS) is the sum of the scores of steatosis (0-3), hepatocyte ballooning (0-2), and lobular inflammation (0-3). To calculate the NAS, H&E-stained images (×20) were analyzed and scored, according to the criteria of Brunt et al.,[11] by a trained hepatopathologist who was blinded to the sample groupings.

ANALYSIS OF MOUSE HEPATIC LIPIDS

Liver tissue triglyceride, total cholesterol (TC), and nonesterified fatty acid (NEFA) were measured using commercial kits (290-63701 for the triglyceride assay, 294-65801 for the TC assay, and 294-63601 for the NEFA assay; Wako, Osaka, Japan).

IN VITRO CELL MODEL OF LIPID ACCUMULATION

PA (P0500; Sigma-Aldrich) was dissolved in 0.01 M NaOH to make a stock solution. PA stock was diluted by adding the indicated culture medium with 25% bovine serum albumin (BSA; BAH66-0050; Equitech-Bio) to obtain a PA solution. Oleic acid (OA; O1008; Sigma) was dissolved in 0.01 M NaOH to an indicated concentration. For the oil red O staining assay, PA and OA stock solutions and 25% BSA were mixed and diluted with medium to the concentration indicated in the figure legends. Cells were stained with 60% oil red O (O1391; Sigma) working solution for 10 minutes to visualize the amount of lipid accumulation. Intracellular triglyceride levels were measured using a commercially available kit (Triglyceride Colorimetric Assay Kit, 10010303; Cayman) following the manufacturer's protocol.

QUANTITATIVE RT-PCR

Total mRNA was extracted from tissues and cultured cells using TRIzol (15596-026; Invitrogen) and converted to cDNA using oligo (dT) primers with the Transcriptor First Strand cDNA Synthesis Kit (04896866001; Roche). Quantitative real-time PCR was performed with SYBR Green (04887352001; Roche). The mRNA expression of related genes was normalized against that of β-actin. The primers used for real-time PCR are shown in Supporting Table S3.

MOUSE EXPERIMENTS

During the experiments, body weight, fasting blood glucose (FBG), and fasting serum insulin (FINS) were determined at different time points. After the mice had fasted for 6 hours, FBG and FINS were determined using a glucometer and enzyme-linked immunosorbent assay, respectively. Based on the measurements of FBG and FINS, the IR index (homeostasis model assessment of insulin resistance [HOMA-IR]) was calculated as follows: [FBG (mmol/L) × FINS (mIU/L)]/22.5. For the glucose tolerance test (GTT), mice were intraperitoneally injected with 1 g/kg glucose after a 6-hour fast, whereas for the insulin tolerance test (ITT), 0.75 U/kg insulin was intraperitoneally injected after a 6-hour fast. The blood glucose concentration in tail blood was detected using a glucometer at baseline and 15, 30, 60, and 120 minutes after injection. The area under the curve (AUC) is given as the incremental AUC (area above baseline), calculated by the conventional trapezoid rule.

LIVER FUNCTION ASSAY

Liver function was evaluated by determining the serum concentrations of alanine aminotransferase (ALT), aspartate aminotransferase (AST), and alkaline phosphatase (ALP) using an ADVIA 2400 Chemistry System analyzer (Siemens, Tarrytown, NY), according to the manufacturer's instructions.

IMMUNOFLUORESCENCE STAINING

For immunofluorescence microscopy, paraffin sections were labeled with primary antibodies overnight and incubated with a suitable fluorophore-conjugated secondary antibody for 1 hour. Rabbit anti-mouse-CD11b antibody (ab75476, 1:100; Abcam) and rat anti-mouse-Ly6G antibody (551459, 1:25; BD) were used to stain infiltrated inflammatory cells, neutrophils, macrophages, and Kupffer cells in liver sections.

Immunofluorescence images were obtained using a fluorescence microscope with DP2-BSW software (version 2.2; Olympus). Positively stained cells in the images were quantified using Image-Pro Plus software.

CELL LINES

The human normal hepatocyte cell line L-02 and HEK293T cells were purchased from the Type Culture Collection of the Chinese Academy of Sciences (Shanghai, China). All cell lines in our laboratory are passaged no more than 30 times after resuscitation and routinely tested for mycoplasma contamination using PCR. Cells were cultured in standard medium containing DMEM, 10% fetal bovine serum, and 1% penicillin–streptomycin and placed in 5% CO_2 under a water-saturated atmosphere in a cell incubator at 37°C.

PLASMID CONSTRUCTS

Full-length sequences of the human Dusp9 coding region were subcloned into pcDNA5–hemagglutinin (HA) and phage-Flag vectors to generate the pcDNA5-HA-Dusp9 and phage-Flag-Dusp9 recombinant plasmids. The Dusp9 coding region was cloned into a vector that contained glutathione *S*-transferase (GST)-HA to create GST-HA-Dusp9. Dusp9 truncations (1-200 and 201-384 amino acids) were obtained through PCR amplification. The products of the Dusp9 truncations were digested with corresponding enzymes and ligated into pcDNA5-Flag to obtain the corresponding plasmids. Using the same method, the pcDNA5-HA-apoptosis signal–regulating kinase 1 (ASK1), pcDNA5-Flag-ASK1, and Flag-labeled ASK1 truncations (1-678, 679-936, and 937-1374 amino acids, respectively) were constructed. The primers used to generate these constructs are listed in Supporting Table S4.

IMMUNOPRECIPITATION

Immunoprecipitation (IP) was performed to determine protein–protein interactions. For co-IP, HEK293T cells were cotransfected with the indicated plasmids. After transfection for 24 hours, cells were washed with cold phosphate-buffered saline and homogenized in ice-cold IP buffer (20 mM Tris-HCl, pH 7.4, 150 mM NaCl, 1 mM ethylene diamine tetraacetic acid, and 0.5% Nonidet P40) containing protease inhibitor cocktail (04693132001; Roche), followed by centrifugation at 12,000 g for 10 minutes. The obtained cell lysates were precleared with protein A/G-agarose beads (11719394001 and 11719386001; Roche) for 3 hours and incubated with the indicated antibody at 4°C overnight. The immunoprecipitated proteins were washed 5-6 times with IP buffer, boiled with SDS loading buffer, separated on SDS-PAGE, and subjected to immunoblotting using the indicated primary antibodies and the corresponding secondary antibodies.

GST PRECIPITATION ASSAYS

Direct interaction between Dusp9 and ASK1 was detected using GST precipitation assays. Briefly, Rosetta (DE3) *Escherichia coli* were transformed with the vector pGEX-4T-1-GST-Dusp9, and vector expression was induced using 0.5 mM isopropyl-β-D-thiogalactopyranoside. The *E. coli* were lysed, and the extracts were incubated with glutathione-sepharose 4B beads at 4°C for 1 hour. The beads were incubated with purified Flag-tagged ASK1, which was prepared through IP, for an additional 4 hours. Proteins that interacted with GST-Dusp9 were eluted in elution buffer (50 mM Tris-HCl, pH 8.0, and 20 mM reduced glutathione) and subjected to immunoblotting using anti-Flag antibodies. Extracts from *E. coli* that expressed the GST tag alone were used as the negative control.

ADENOVIRUS VECTOR CONSTRUCTION

A dominant-negative mutation plasmid was obtained to construct AddnASK1 adenoviruses as reported.[12] Adenoviral green fluorescent protein (AdGFP) was used as a control. Recombinant adenoviruses were generated using the AdEasy Vector Kit. Plasmids were recombined with the pAdEasy backbone vector, according to the manufacturer's instructions, and transfected into 293A using FuGENE transfection reagent. Recombinant adenoviruses were plaque-purified, tittered to 10^9 plaque-forming units/mL, and verified through restriction digestion. Primary hepatocytes were infected with the indicated adenoviruses in diluted medium at a multiplicity of infection of 50 for 24 hours.

STATISTICAL ANALYSIS

All data are presented as the means ± SD. Differences between two groups were determined using a two-tailed Student *t* test, and differences among three groups or more were evaluated by one-way analysis of variance (ANOVA), followed by Tukey's *post hoc* test for data meeting homogeneity of variance or with Tamhane's T2 analysis for data of heteroscedasticity. $P < 0.05$ was considered statistically significant.

Results

HEPATIC Dusp9 EXPRESSION IS DECREASED IN NAFLD

To determine the relevance of Dusp9 in hepatic metabolism, we measured its expression in liver samples from HFD-induced or *ob/ob* mice. Expression of Dusp9 was down-regulated in a time-dependent manner (Fig. 1A,B). To determine whether this decrease occurred in hepatocytes, primary cells were isolated from wild-type (WT) mice and stimulated with vehicle or PA, an inducer of lipid accumulation and IR in hepatocytes.[13] Compared with vehicle-treated cells, PA triggered a marked decrease in Dusp9 expression in hepatocytes (Fig. 1C). Immunohistochemistry also revealed that Dusp9 expression was decreased in the livers of mice on the HFD for 24 weeks (Fig. 1D). In contrast, our results showed that the Dusp9 mRNA levels were no different in the liver (and hepatocytes) between the HFD and control groups, both *in vivo* and *in vitro* (Supporting Fig. S1A,B). Taken together, these results suggest that Dusp9 may play a role in the development of obesity-associated pathologies.

HEPATIC Dusp9 DEFICIENCY EXACERBATES HFD-INDUCED OBESITY AND HEPATIC STEATOSIS

The effects of Dusp9 deficiency in NAFLD were examined in Dusp9-CKO mice (Fig. 2A-D). After continuous administration of the HFD for 24 weeks,

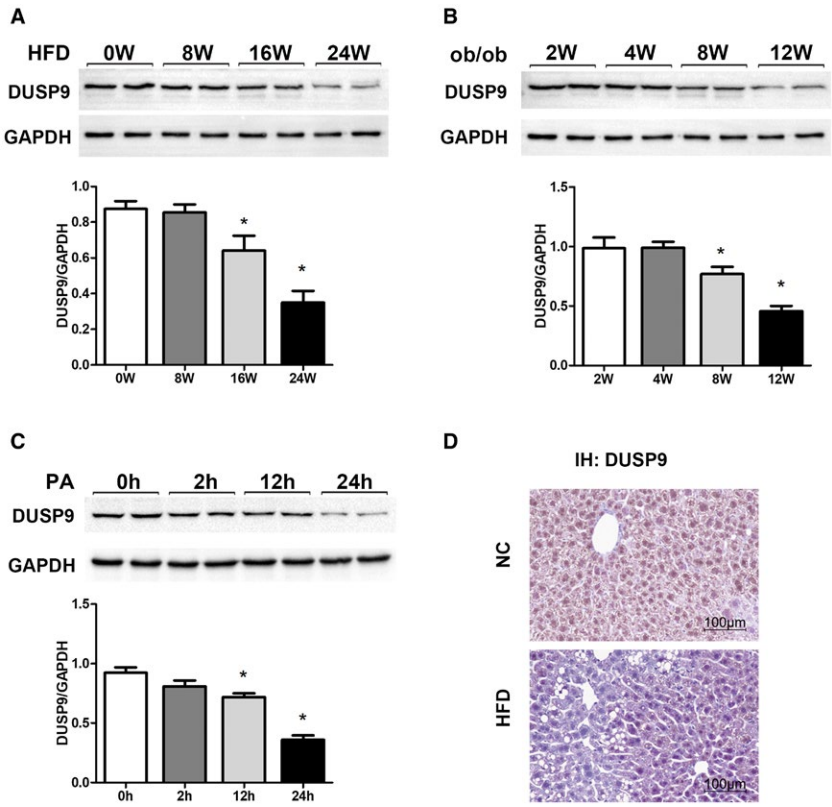

FIG. 1. Dusp9 expression is down-regulated in livers with hepatic steatosis. (A) Dusp9 protein expression in the liver of WT mice after different weeks of NCD or HFD (n = 4), **P* < 0.05 versus NCD-fed mice. (B) Dusp9 protein expression in the liver of *ob/ob* mice (n = 4), **P* < 0.05 versus 2-week-old mice. (C) Dusp9 protein expression in primary hepatocytes, which were isolated and stimulated with PA (0.3 mM) for 24 hours (n = 4). The data represent mean ± SD. **P* < 0.05 versus vehicle control. (D) Dusp9 expression by immunohistochemistry in the livers of 24-week-old HFD mice. Scale bar, 100 μm (n = 4). Statistical analysis was carried out by the Student two-tailed *t* test. Abbreviations: IH, immunohistochemistry; NC, normal chow.

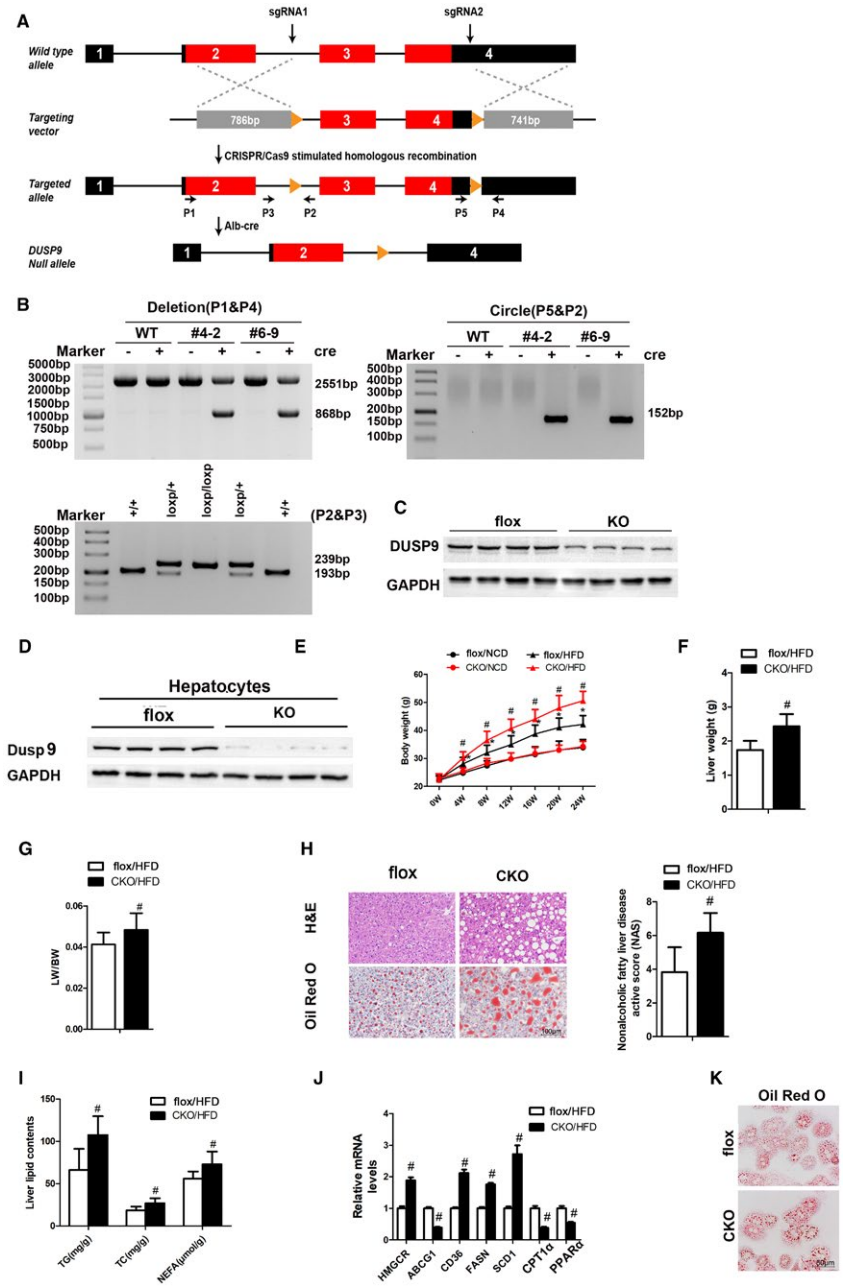

FIG. 2. Liver-specific Dusp9 deficiency exacerbates HFD-induced obesity and hepatic steatosis. (A) Schematic image of the generation of a liver-specific Dusp9-KO mouse (Dusp9-CKO) strain. (B) Mouse genotyping was confirmed by PCR. (C) Dusp9 protein expression in the liver of Dusp9-flox and Dusp9-CKO mice. (D) Dusp9 expression in hepatocytes isolated from Dusp9-flox and Dusp9-CKO mice. (E) Changes in the body weight of Dusp9-CKO and Dusp9-flox mice treated with the HFD or NCD for 24 weeks (n = 10). (F,G) Liver weights (F) and the LW/BW ratio (G) of Dusp9-CKO and Dusp9-flox mice at 24 weeks post-HFD administration (n = 10). (H) H&E (upper) and oil red O (bottom) staining of liver sections of Dusp9-CKO and Dusp9-flox controls after HFD treatment (n = 10). Scale bar, 100 μm. (I) Hepatic triglyceride, TC, and NEFA contents of mice in the indicated groups were measured by commercial kits (n = 10). (J) mRNA expression of genes related to cholesterol synthesis and efflux and fatty acid uptake and synthesis in the liver samples of Dusp9-flox and Dusp9-CKO mice after HFD treatment for 24 weeks (n = 4). (K) Lipid accumulation displayed by oil red O staining in primary hepatocytes from Dusp9-CKO and Dusp9-flox mice subjected to PA administration for 24 hours (n = 10). Scale bar, 50 μm. The data represent mean ± SD. $^{*}P < 0.05$ versus Dusp9-flox/NCD group, $^{\#}P < 0.05$ versus Dusp9-flox/HFD group. For statistical analysis, a two-tailed Student *t* test was used for (F-J) and one-way ANOVA was used for (E). Abbreviations: Cas9, CRISPR-associated 9; CRISPR, clustered regularly interspaced short palindromic repeats; sgRNA, single-guide RNA.

the body weight, liver weight, and ratio of liver-to-body weight (LW/BW) were gradually increased in the Dusp9-flox control group of mice, whereas the increase was more evident in the CKO mice (Fig. 2E-G). Furthermore, in the HFD-fed Dusp9-CKO mice, lipid accumulation and content in the liver were significantly increased, as indicated by H&E-stained and oil red O–stained liver sections (Fig. 2H) and hepatic triglyceride, TC, and NEFA levels (Fig. 2I). Moreover, the results showed that the mRNA expression of genes involved in cholesterol synthesis (3-hydroxy-3-methylglutaryl coenzyme A reductase [HMGCR]), fatty acid uptake (cluster of differentiation 36 [CD36]), and fatty acid synthesis (fatty acid synthase [FASN], stearoyl-CoA desaturase-1 [SCD1]) in the liver was significantly up-regulated, whereas the gene expression of adenosine triphosphate–binding cassette transporter G1 (ABCG1), carnitine palmitoyltransferase 1 (CPT1α), and peroxisome proliferator–activated receptor alpha (PPARα) was much lower in the CKO mice than in the Dusp9-flox controls after HFD treatment for 24 weeks (Fig. 2J). *In vitro*, there was a greater accumulation of lipids in Dusp9-CKO primary hepatocytes than in Dusp9-flox controls after stimulation with a PA and OA mixture for 24 hours (Fig. 2K).

HEPATIC Dusp9-TRANSGENIC MICE ARE TOLERANT TO HFD-INDUCED OBESITY AND HEPATIC STEATOSIS

In addition to the loss-of-function approach, Dusp9-TG were established (Supporting Fig. S2A) to determine whether Dusp9 overexpression in the liver could attenuate HFD-induced NAFLD and related metabolic disorders. Expression of Dusp9 was elevated in the liver (Supporting Fig. S2B), and the mice (TG4) with the highest Dusp9 levels were used for subsequent experiments. The Dusp9-TG mice and their age-matched control littermates were fed the NCD or HFD for 24 weeks. The HFD induced a more pronounced increase in body weight in the control mice than in the Dusp9-TG mice, whereas no obvious difference in body weight was noted between the two groups fed the NCD (Supporting Fig. S2C). The Dusp9-TG mice had a lower liver weight and LW/BW ratio compared to the control mice (Supporting Fig. S2D,E). In HFD-fed Dusp9-TG mice, lipid accumulation and content in the liver were significantly decreased, as indicated by H&E-stained and oil red O–stained liver sections (Supporting Fig. S2F) and hepatic triglyceride, TC, and NEFA levels (Supporting Fig. S2G). Moreover, RT-PCR showed that the mRNA expression of HMGCR, CD36, FASN, and SCD1 in the liver was significantly inhibited by Dusp9 overexpression, whereas the gene expression of ABCG1, CPT1α, and PPARα was much higher in the Dusp9-TG mice than in the controls after HFD treatment for 24 weeks (Supporting Fig. S2H).

HEPATIC Dusp9 BLUNTS HFD-INDUCED IR

HFD-induced Dusp9-CKO mice had consistently higher fasting glucose levels, plasma insulin levels, and HOMA-IR indexes than their Dusp9-flox counterparts (Fig. 3A-C). Additionally, compared with the Dusp9-flox mice, glucose tolerance was decreased and insulin sensitivity compromised in the CKO mice, as shown by the intraperitoneal GTT and ITT (Fig. 3D,E). Coincident with this metabolic dysfunction phenotype, the expression of genes related to gluconeogenesis (phosphoenolpyruvate carboxykinase 1 [PCK1] and glucose-6-phosphatase catalytic subunit [G6PC]) was higher in the Dusp9-CKO mice than in the Dusp9-flox controls (Fig. 3F). These data indicate that hepatic Dusp9 plays an important role in the regulation of insulin sensitivity in mice. The insulin-related insulin receptor substrate 1 (IRS1)/AKT/glycogen synthase kinase 3 beta (GSK3β) signaling pathways were examined by western blotting, and the results demonstrated that the expression of phosphorylated IRS1, AKT, and GSK3β was considerably decreased in the livers of Dusp9-CKO mice compared with Dusp9-flox mice (Fig. 3G).

Similarly, after HFD treatment, fasting glucose and insulin levels were markedly lower (with a lower HOMA-IR index) in the HFD-fed Dusp9-TG mice than in the control mice (Supporting Fig. S3A-C). The GTT and ITT assays revealed that glucose tolerance and insulin sensitivity were significantly enhanced in the HFD-fed Dusp9-TG mice compared with the controls (Supporting Fig. S3D,E). Furthermore, analysis of the gluconeogenesis-related genes PCK1 and G6PC indicated that the activation level of these components in the liver was lower in

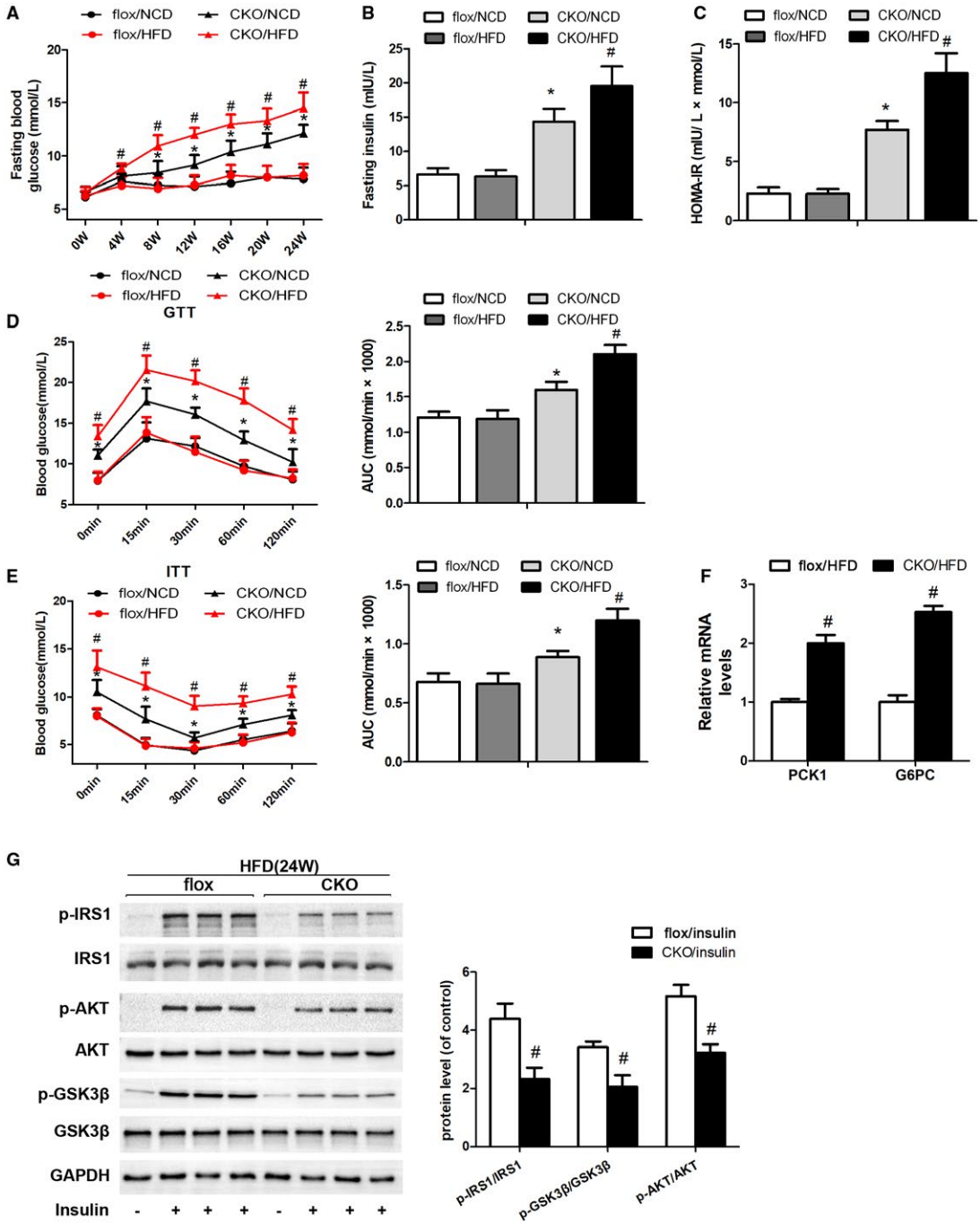

FIG. 3. Liver-specific Dusp9 deficiency exacerbates insulin resistance. (A-C) Fasting blood glucose (A), fasting insulin (B), and HOMA-IR (C) in Dusp9-CKO or Dusp9-flox mice treated with the HFD or NC for 24 weeks. FBG levels were measured every 4 weeks. FINS was measured at the endpoint of this experiment. (D,E) Intraperitoneal GTT (1 g/kg) (D) and intraperitoneal ITT (0.75 units/kg) (E) were performed on Dusp9-flox and Dusp9-CKO mice at week 22 or 23 of food administration, respectively. The corresponding AUC of blood glucose level was calculated (n = 10). (F) mRNA levels of PCK1 and G6PC in the liver from mice in the indicated groups (n = 4). (G) Representative western blot showing levels of total and phosphorylated IRS1, AKT, and GSK3β in the livers of Dusp9-flox and Dusp9-CKO mice fed the HFD for 24 weeks; some mice received intraperitoneal insulin injection 10 minutes before liver tissue collection. GAPDH serves as the internal control (n = 4). $^{*}P < 0.05$ versus Dusp9-flox /NCD group, $^{\#}P < 0.05$ versus Dusp9-flox/HFD group. The data represent mean ± SD. Significance was determined by one-way ANOVA (A-E) and Student two-tailed *t* test (F,G). Abbreviation: p-, phosphorylated.

the Dusp9-TG mice than in the control mice. These results indicate that increased expression of Dusp9 in hepatocytes attenuates HFD-induced IR.

HEPATIC Dusp9 BLUNTS THE HFD-INDUCED HEPATIC INFLAMMATORY RESPONSE

Given the close association among obesity, IR, hepatic steatosis, and inflammation, we examined the effect of Dusp9 on hepatic inflammatory response. The mRNA levels of proinflammatory cytokines (tumor necrosis factor-alpha [TNF-α], interleukins 1β and 6) and chemokines (chemokine [C-C motif] ligands 5 and 2) were significantly higher in Dusp9-CKO mice but lower in Dusp9-TG mice than in their corresponding controls after HFD treatment (Fig. 4A,B). Excessive activation of inhibitor of nuclear factor kappa B kinase subunit beta (IKK-β)/nuclear factor kappa B (NF-κB) in mice reportedly contributed to hepatic IR and elevated hepatic production of inflammatory cytokines.[14] Thus, we assessed whether this axis is regulated by Dusp9 during HFD-induced hepatic steatosis and related pathologies. In Dusp9-CKO mice, activation of IKK-β, P65, and inhibitor of κBα in response to the HFD was significantly enhanced compared with that in Dusp9-flox mice (Fig. 4C,D). However, Dusp9-TG mice displayed blunted activation of IKK-β/NF-κB signaling compared with the control mice. In addition, Dusp9-CKO mice had more serious liver injury than Dusp9-flox control mice, whereas Dusp9-TG mice exhibited better liver function, as evidenced by serum ALT, AST, and ALP levels. (Fig. 4E,F).

HEPATIC Dusp9 DEFICIENCY EXACERBATES HFHC-INDUCED LIVER FIBROSIS AND INFLAMMATION

To mimic NASH in human pathophysiology, an HFHC diet mouse model was constructed.[15] In the Dusp9-CKO mice, body weight, liver weight, and LW/BW ratio were all increased following the HFHC diet compared with the Dusp9-flox mice on the same diet (Fig. 5A). FBG, hepatic lipid accumulation, collagen deposition, and NAS (Fig. 5B,C) were also significantly higher in Dusp9-CKO mice than in Dusp9-flox mice. In addition, immunostaining demonstrated that inflammatory cells infiltrating the liver were more pronounced in Dusp9-CKO mice than in controls (Fig. 5D). Consistent with this finding, mRNA levels of inflammatory markers were significantly higher in the livers of Dusp9-CKO mice (Fig. 5E). Notably, the expression of NASH-related profibrotic genes in the liver was significantly higher in Dusp9-CKO mice than in controls (Fig. 5F). In addition, Dusp9-CKO mice exhibited more serious liver injury, as evidenced by the higher serum ALT and AST levels compared to Dusp9-flox mice (Fig. 5G). These results indicate that liver Dusp9 deficiency exacerbates HFHC-induced liver inflammation and fibrosis.

Dusp9 WEAKENS THE ACTIVATION OF ASK1–P38/JNK SIGNALING

Dusp9 contributes to the regulation of MAPK signaling, which is intimately involved in the pathogenesis of several metabolic disorders.[16] This relationship prompted us to investigate whether the MAPK pathway participates in Dusp9-regulated hepatic steatosis. The phosphorylation of ERK1/2, JNK, and p38 was increased in liver samples from all HFD-fed groups and primary hepatocytes stimulated with PA compared with that in liver samples from the NCD groups. However, only the phosphorylation of JNK and p38 was affected by Dusp9 modulation. Dusp9 overexpression greatly attenuated and Dusp9 deficiency markedly enhanced the phosphorylation of JNK and p38 compared with the corresponding controls (Fig. 6A,B). To explore the possible upstream factors of the Dusp9-mediated activation of JNK and p38, we measured the activation of several signaling molecules, including TANK binding kinase 1 (TBK1), ASK1, and MAPK kinase 4/7 (MKK4/7), which regulate MAPKs in various physiological processes.[16,17] HFD treatment or PA challenge enhanced the activation of these proteins, whereas the activity of ASK1 and its downstream targets MKK4/7 was markedly promoted by Dusp9 deficiency and strongly inhibited by Dusp9 overexpression compared with the corresponding controls (Fig. 6C,D). These findings suggest that the ASK1–MKK4/7–p38/JNK signaling pathway is regulated by Dusp9 during hepatic steatosis and related metabolic disorders.

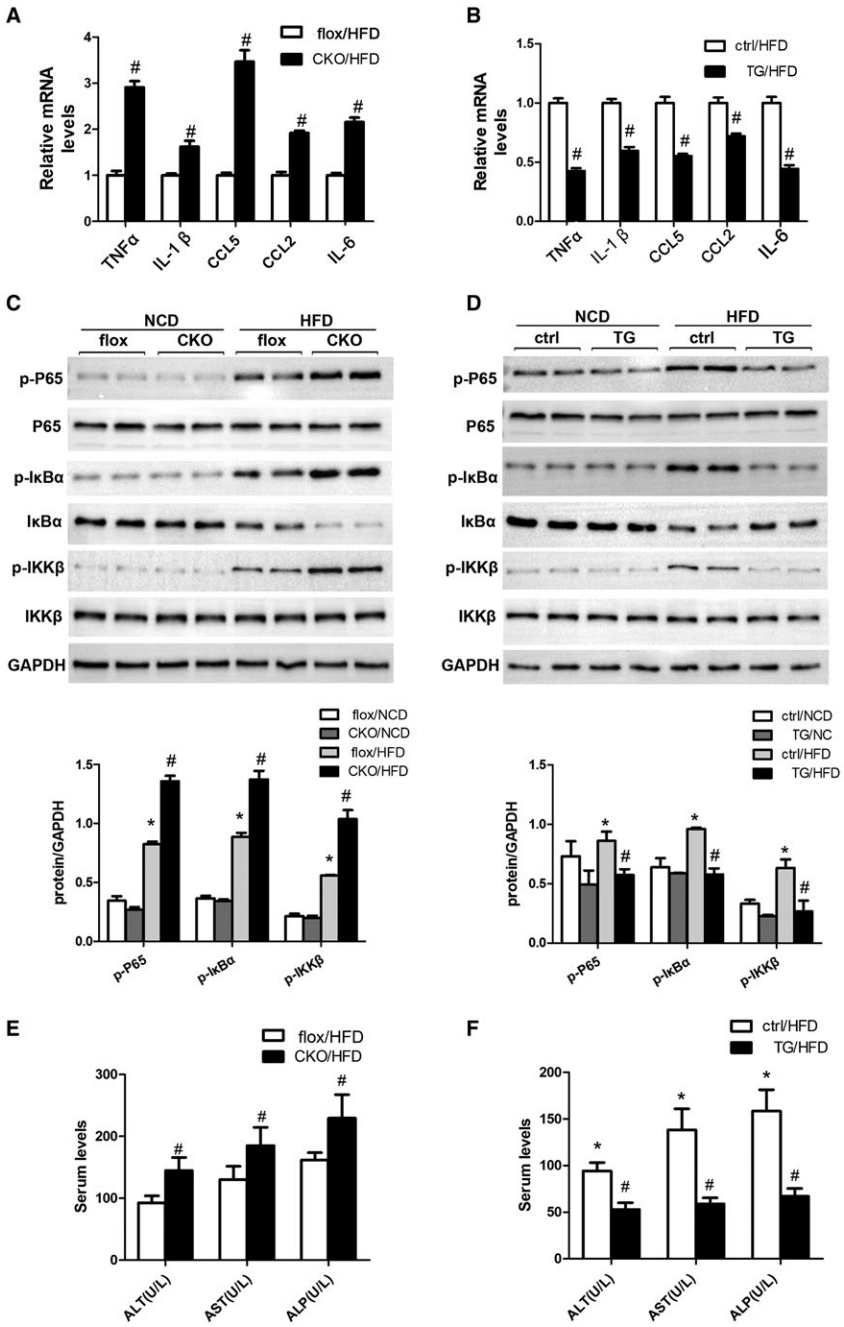

FIG. 4. HFD-induced hepatic inflammatory response can be significantly blunted by Dusp9 in hepatocytes. (A,B) mRNA expression levels of inflammatory cytokines and chemokines in the liver of indicated groups (n = 4). (C,D) Expression of key proteins in NF-κB signaling in the liver of Dusp9-CKO mice, Dusp9-TG mice, and their corresponding littermate controls after HFD or NC treatment for 24 weeks. Protein expression was normalized to that of GAPDH (n = 4). (E,F) Serum concentrations of ALT, AST, and ALP in Dusp9-CKO mice, Dusp9-TG mice, and their corresponding littermate controls after HFD or NC treatment for 24 weeks (n = 10 mice per group). The data represent mean ± SD. (A-F) $^{*}P < 0.05$ versus Dusp9-flox/NCD group, $^{\#}P < 0.05$ versus Dusp9-flox/HFD group. Significance was determined by Student two-tailed *t* test (A,B,E,F) and one-way ANOVA (C,D). Abbreviations: CCL, chemokine (C-C motif) ligand; IL, interleukin; p-, phosphorylated.

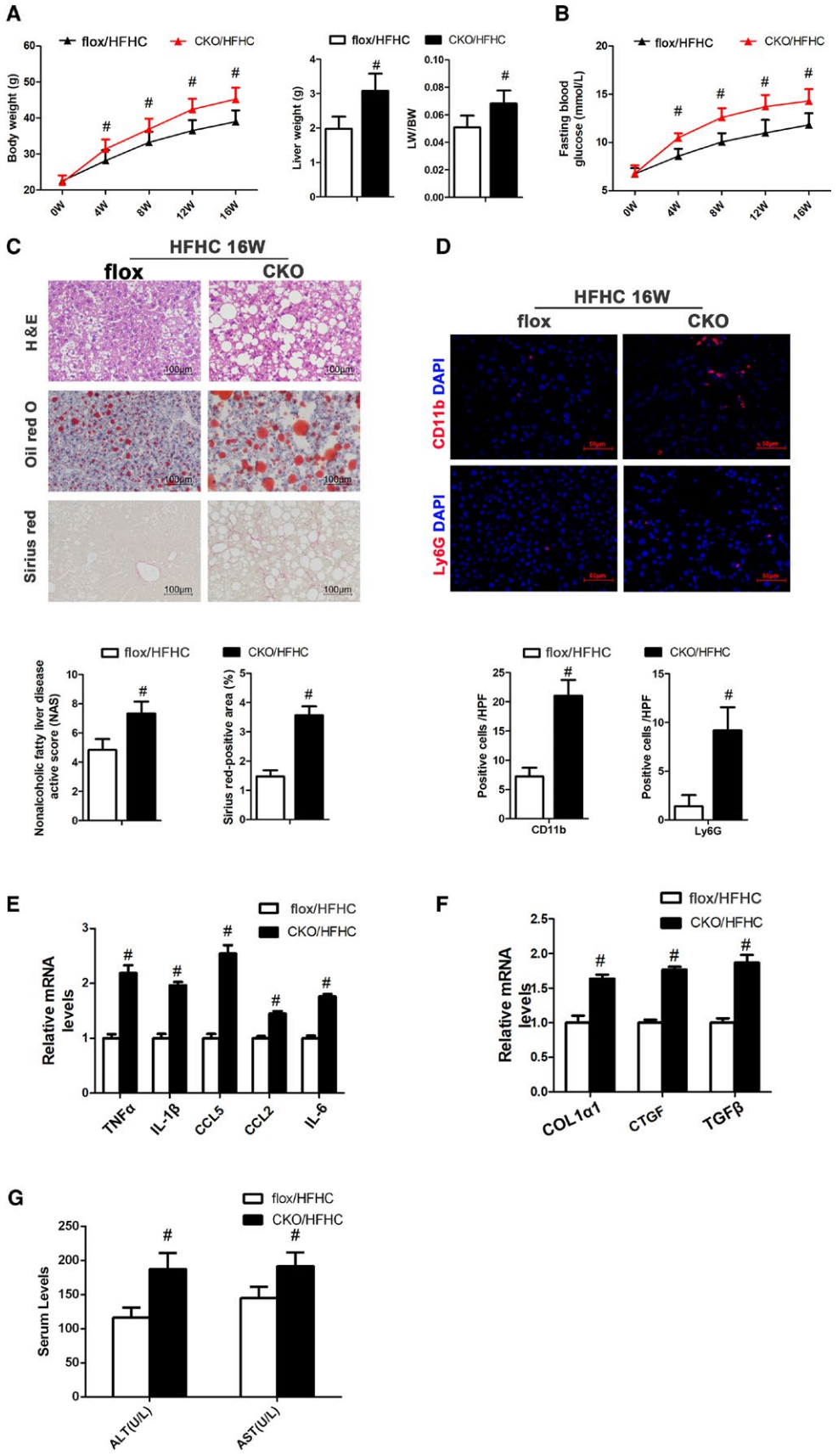
A
flox/HFHC
CKO/HFHC
Body weight (g)
0W
4W
8W
12W
16W
Liver weight (g)
LW/BW
B
Fasting blood glucose (mmol/L)
C
HFHC 16W
flox
CKO
H&E
Oil red O
Sirius red
100μm
D
CD11b DAPI
Ly6G DAPI
Nonalcoholic fatty liver disease active score (NAS)
Sirius red-positive area (%)
Positive cells /HPF
CD11b
Ly6G
E
Relative mRNA levels
TNFα
IL-1β
CCL5
CCL2
IL-6
F
COL1α1
CTGF
TGFβ
G
Serum Levels
ALT(U/L)
AST(U/L)

FIG. 5. Hepatocyte Dusp9 aggravates lipid accumulation, inflammation, and fibrosis, thus accelerating NASH progression. (A) Changes in body weight, liver weight, and LW/BW ratio of Dusp9-CKO and Dusp9-flox mice treated with the HFHC diet for 16 weeks (n = 10). FBG in Dusp9-CKO or Dusp9-flox mice treated with the HFHC diet for 16 weeks. FBG levels were measured every 4 weeks. (C) Representative images of H&E-stained (top) oil red O–stained (middle), and picrosirius red–stained (bottom) liver sections from the indicated mice fed the HFHC diet for 16 weeks (n = 10, with 10 images for each mouse). Scale bar, 100 μm. NAS (left) and fibrotic area (right) of Dusp9-flox and Dusp9-CKO mice fed the HFHC diet for 16 weeks (n = 10). (D) Representative images showing immunofluorescence staining for CD11b (top, red) and Ly6G (bottom, red) in the livers of the indicated mice fed the HFD for 16 weeks. Nuclei were labeled with 4′,6-diamidino-2-phenylindole (blue) (n = 4 mice, with 10 images for each mouse). Scale bar, 50 μm. And the numbers of CD11b-positive and Ly6G-positive cells were averaged in each high-power field. (E,F) mRNA levels of proinflammatory (E) and profibrotic (F) genes in the liver from mice in the indicated groups (n = 4). mRNA expression of target genes was normalized to that of β-actin. (G) Serum concentrations of ALT and AST in Dusp9-flox and Dusp9-CKO mice fed the HFHC diet for 16 weeks (n = 10). $^{\#}P < 0.05$ versus Dusp9-flox/HFHC group. The data represent mean ± SD. Significance was determined by Student two-tailed *t* test (A-G). Abbreviations: CCL, chemokine (C-C motif) ligand; COL1α1, collagen type 1 alpha 1; CTGF, connective tissue growth factor; DAPI, 4′,6-diamidino-2-phenylindole; HPF, high-power field; IL, interleukin; TGFβ, transforming growth factor beta.

DUSP9 BINDS TO ASK1 AND BLOCKS ITS PHOSPHORYLATION

To verify that Dusp9 directly interacts with ASK1, we performed a series of IP experiments using the HEK293T cell line. IP experiments demonstrated that Dusp9 coimmunoprecipitated with ASK1 (Fig. 7A,B). A GST-tagged Dusp9 efficiently pulled down ASK1 (Fig. 7C). These results suggest that Dusp9 works directly with ASK1. Next, we created serially truncated forms of Dusp9 and ASK1 and performed co-IP assays to identify what regions of Dusp9 and ASK1 mediate the interaction. The mapping results showed that the domain encompassing amino acids 201-384 on Dusp9 bound to the domain encompassing amino acids 1-678 on ASK1 (Fig. 7D,E). To verify the effect of Dusp9 on ASK1 signaling, equal amounts of Flag-ASK1 and HA-Dusp9 at various concentrations were transferred to the normal hepatic cell line L-02, and the results showed that Dusp9 inhibited the phosphorylation of ASK1 in a dose-dependent manner (Fig. 7F).

BLOCKING ASK1 ATTENUATES DUSP9-REGULATED HEPATIC STEATOSIS AND INFLAMMATION

To further demonstrate that the suppression of ASK1 signaling is responsible for the protective effect of Dusp9, we blocked ASK1 activity by introducing ASK1 with the phosphorylation locus silenced into primary mouse hepatocytes from WT and Dusp9-CKO mice (Fig. 8A). We found that in primary hepatocytes stimulated with PA, blocking ASK1 activity almost completely inhibited the lipid accumulation potentiated by Dusp9 knockout (Fig. 8B,C). Similarly, blocking ASK1 activity suppressed the up-regulated mRNA expression of lipid metabolism and inflammatory markers in Dusp9-CKO hepatocytes (Fig. 8D,E). Furthermore, the hyperactivation of downstream p38/JNK signaling that resulted from Dusp9 knockout was inhibited by ASK1 activity blocking (Fig. 8F).

Discussion

Currently, lifestyle changes and weight loss are the only therapeutic options for the management of NAFLD and NASH. While clinical trials showed that several agents, such as obeticholic acid, can improve NAFLD, pioglitazone (Actos), a medicine for type 2 diabetes, was found to ameliorate NASH in individuals who did not have diabetes.[18] To date, no medications for NAFLD have been approved by relevant governmental agencies.[19] In this study, we attempted to discover a target for the treatment of NAFLD and NASH and showed that Dusp9 was a key suppressor for HFD-induced hepatic steatosis and inflammatory responses. Moreover, we also demonstrated that Dusp9 deficiency aggravated HFHC-induced liver fibrosis. Finally, our study demonstrated that Dusp9 exerted its effects by blocking ASK1 phosphorylation and the subsequent activation of p38 and JNK signaling. These findings suggest that Dusp9 may be a promising therapeutic target for the treatment of NAFLD and NASH.

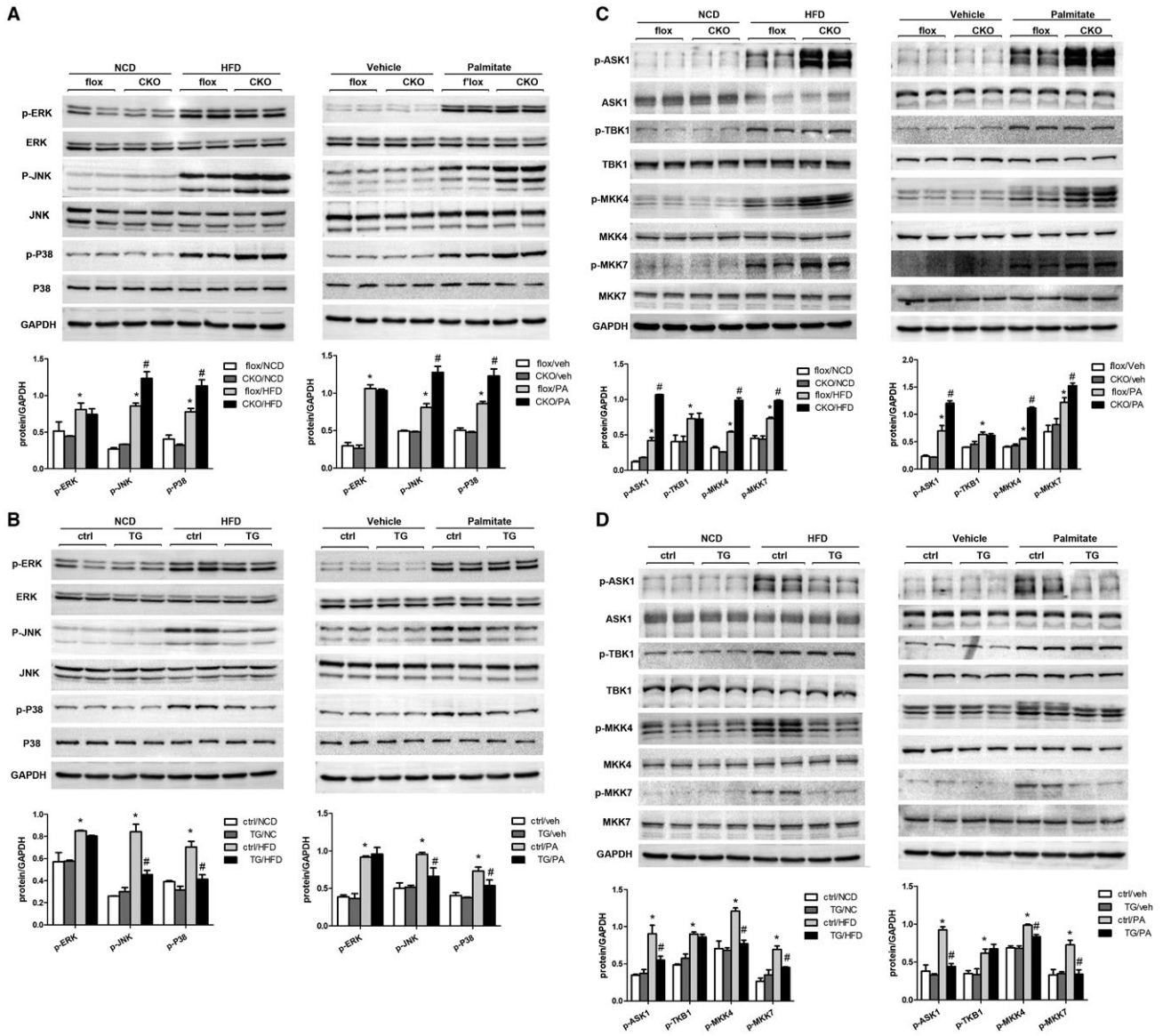

FIG. 6. ASK1 and its downstream pathways are involved in Dusp9-regulated hepatic steatosis. (A,B) MAPK signaling activation was measured from the total and phosphorylated ERK, JNK, and P38 levels in the livers of Dusp9-CKO (A) or Dusp9-TG (B) mice and their control littermates after HFD treatment for 24 weeks (n = 6) and in primary hepatocytes in the indicated groups after PA (0.3 mM) or vehicle treatment for 24 hours (n = 3 independent experiments). Protein expression was normalized to that of GAPDH. (C,D) JNK and P38 upstream signaling activation was measured from the total and phosphorylated ASK1, TBK1, MKK4, and MKK7 levels in the livers of Dusp9-CKO (C) or Dusp9-TG (D) mice and their control littermates after HFD treatment for 24 weeks (n = 6) and in primary hepatocytes in the indicated groups after PA (0.3 mM) or vehicle treatment for 24 hours (n = 3 independent experiments). Protein expression was normalized to that of GAPDH. $^{*}P < 0.05$ versus Dusp9-flox/NCD, control/NCD, Dusp9-flox/vehicle, or control/vehicle group; $^{\#}P < 0.05$ versus Dusp9-flox/HFD, control/HFD, Dusp9-flox/PA, or control/PA group. The data represent mean ± SD. Significance was determined by one-way ANOVA (A-D).

We observed decreased Dusp9 expression in the fatty liver of mice. In relation to this, Emanuelli et al.[4] reported that Dusp9 mRNA was up-regulated in the liver of mice upon HFD feeding. Despite the existing difference, these findings collectively suggested that Dusp9 was closely involved in the metabolic function of liver. We believe that the apparent differences in Dusp9 expression are due

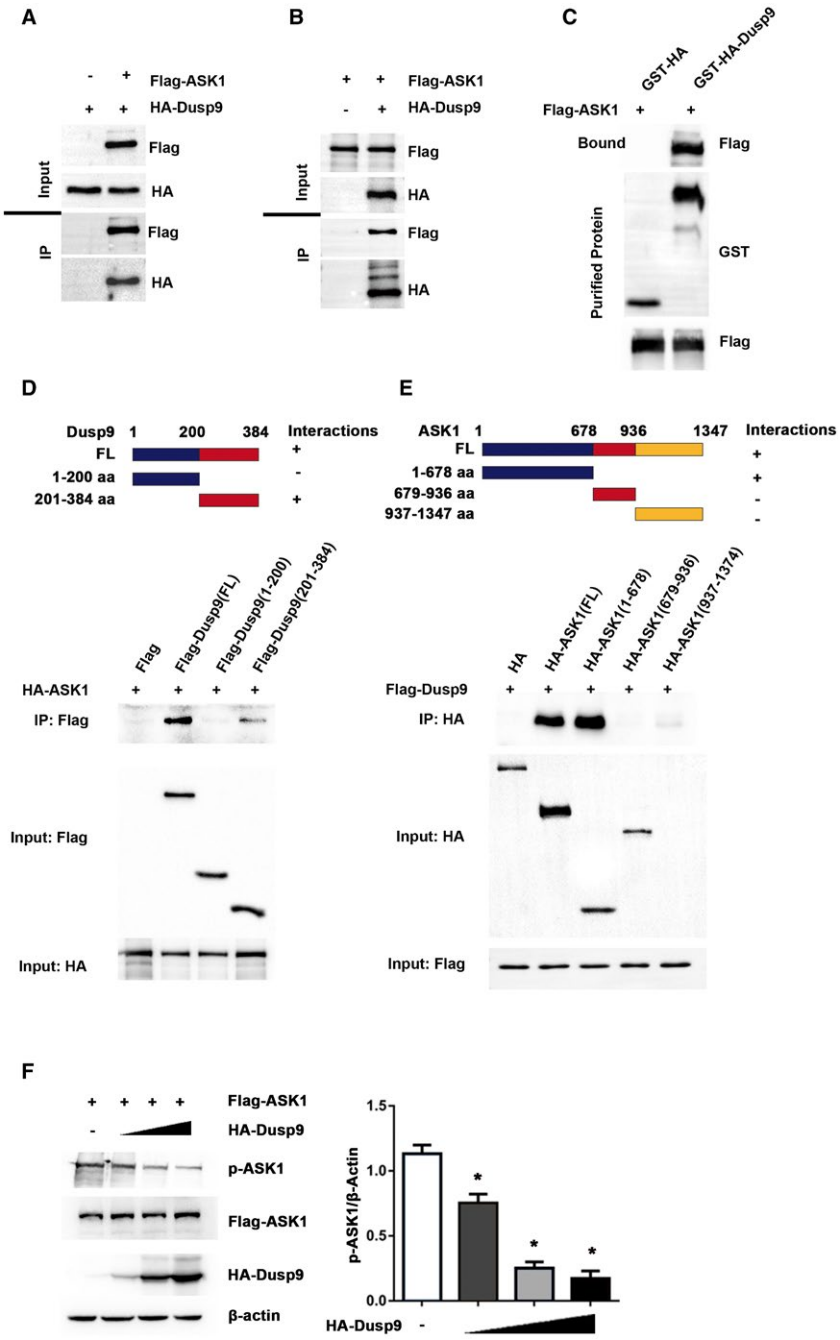

FIG. 7. Dusp9 binds to ASK1 and blocks its phosphorylation. (A,B) A co-IP assay was performed in HEK293T cells cotransfected with Flag-ASK1 and HA-Dusp9 to examine the interaction between ASK1 and Dusp9. (C) GST precipitation assays showing direct Dusp9–ASK1 binding. Purified GST was used as a control. (D,E) The binding domains of Dusp9 and ASK1 were explored using full-length and truncated Dusp9 and ASK1 expression constructs and co-IP assays followed by western blotting. (F) Protein expression of phosphorylated ASK1 was measured in normal hepatic cell line L-02 infected with equal amounts of Flag-ASK1 and a concentration gradient of HA-Dusp9 for 24 hours (n = 3 independent experiments). **P* < 0.05 versus Flag-ASK1 infection group. The data represent mean ± SD. Significance was determined by Student two-tailed *t* test (F). Abbreviations: aa, amino acid; p-, phosphorylated.

to the different experimental conditions used and/or different stages of the disease. At the early time of HFD feeding, as reported by Emanuelli et al.,[4] a compensatory increase of Dusp9 inhibits NAFLD progression. However, relatively long HFD feeding results in decreased Dusp9 expression, which in turn

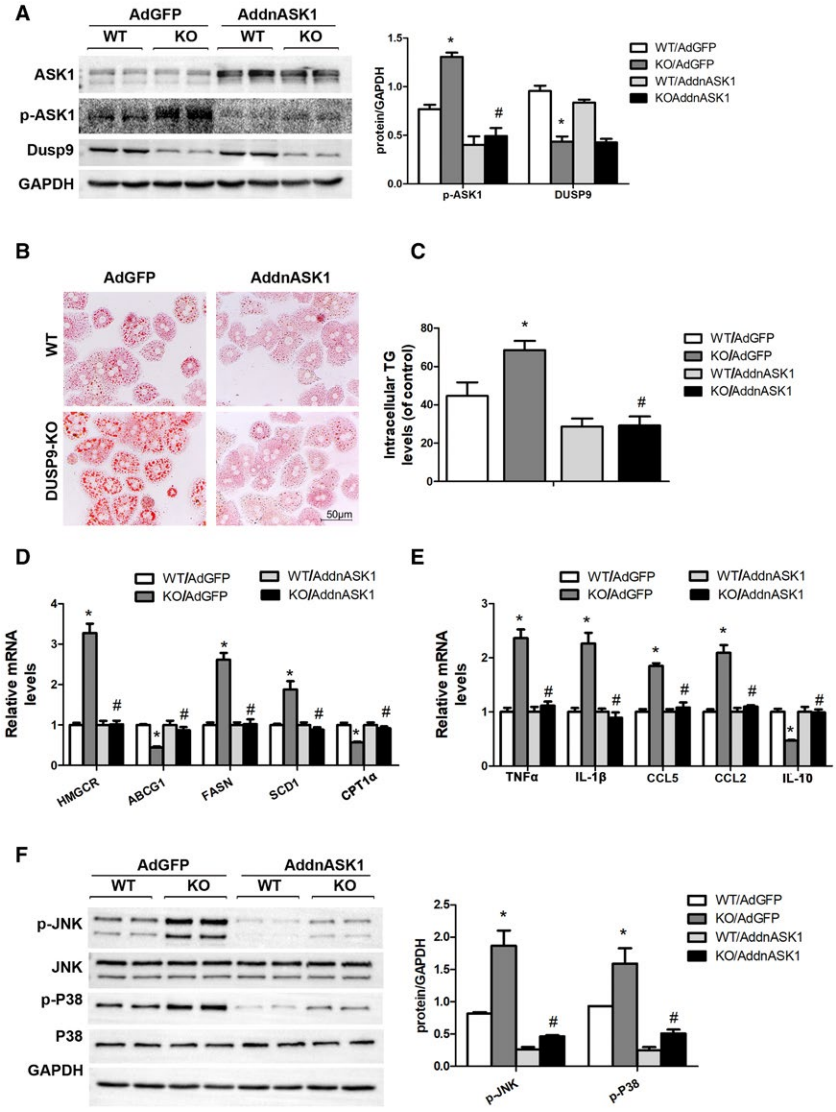

FIG. 8. Blocking ASK1 attenuates Dusp9-regulated hepatic steatosis and inflammation. (A) Protein expression of p-ASK1 and Dusp9 in primary hepatocytes from WT and Dusp9-CKO mice infected with Ad-GFP or Ad-dnASK1 (n = 6). (B,C) Representative oil red O staining (B) and relative intracellular triglyceride levels (C) of primary hepatocytes infected with indicated adenovirus followed by PA stimulation for 24 hours (n = 10). Scale bar, 50 μm. (D,E) mRNA levels of proinflammatory (D) and profibrotic (E) genes in liver from mice in the indicated groups (n = 4). mRNA expression of target genes was normalized to that of β-actin. (F) MAPK signaling activation was measured from the total and phosphorylated JNK and P38 levels in primary hepatocytes in the indicated groups. Protein expression was normalized to that of GAPDH. $^{*}P < 0.05$ versus WT/AdGFP group, $^{\#}P < 0.05$ versus Dusp9-CKO/AdGFP group. The data represent mean ± SD. Significance was determined by one-way ANOVA (A,C-F). Abbreviations: CCL, chemokine (C-C motif) ligand; IL, interleukin; p-, phosphorylated; TG, triglyceride.

aggravates disease. Thus, finding out how Dusp9 expression levels are regulated at different stages of disease is significant and needs further study.

NAFLD is a complex disease, and several pathologic processes including hepatocyte steatosis, IR, inflammation, and fibrosis may be at play in a parallel or sequential fashion along with the whole spectrum of the disease.[20] IR is a major feature of NAFLD and can lead to a vicious cycle of inflammation and fatty acid accumulation in the liver in both humans and rodents.[21] On the other hand, inflammation is a contributor to IR and hepatic steatosis.[22] In the present study, the vicious cycle resulting from hepatocyte steatosis, inflammatory response, IR, and liver fibrosis

was exacerbated by Dusp9 deficiency in hepatocytes. Mechanistically, Dusp9 protects against NASH mainly through restraining ASK1–JNK/p38 signaling. In the liver, JNK/p38 signaling plays a central role in processes that control hepatic metabolism.[23] In brief, JNK1 directly perturbs hepatic lipid metabolism by regulating PPARα[24] and facilitates IR by promoting serine phosphorylation of IRS1 in hepatocytes.[25] Moreover, JNK is closely involved in the hyperactivated inflammatory response in liver.[26] Hepatic p38αβ MAPK has a well-recognized role in regulating glucose homeostasis.[27,28] Thus, Dusp9 achieves its therapeutic potential for NASH by simultaneously maintaining lipid and glucose metabolism homeostasis, improving IR, and decreasing inflammation and fibrosis by regulating ASK1–JNK/p38 signaling.

NAFLD is regarded unquestionably as one of the components of the metabolic syndrome. Hence, metabolic perturbations occurring in the fatty liver can give rise to a systemic metabolic derangement.[29] Hepatocytes are insulin-sensitive cells, and IR in the liver results in profound dysregulation of lipid and glucose metabolism derangement.[30] This study showed that hepatocyte Dusp9 is not functionally confined to the liver but leads to some systemic metabolic disorders, which may be secondary effects of hepatic modulation by Dusp9. Notably, nonparenchymal cells and immune cells also potentially play roles in the pathogenesis of NAFLD and NASH. Whether the Dusp9–Ask1 regulatory axis functions in these other cell types to regulate NASH deserves further investigation. Even so, on the basis of our data, it seems that specific manipulation of the Dusp9–Ask1 pathway in hepatocytes is effective for alleviating NAFLD and NASH.

ASK1 is considered to be the most promising therapeutic target for NASH, especially with the encouraging results from the phase 2 clinical trial of the ASK1 inhibitor selonsertib in treating NASH.[31] Our study revealed that Dusp9 could block the phosphorylation of ASK1 by directly binding to ASK1. Recently, several studies reported that upstream ASK1 regulators could serve as targets for the treatment of NASH. Caspase-8 and Fas-associated protein with death domain–like apoptosis regulator, which blocks the N-terminal dimerization and autophosphorylation of ASK1, could reverse steatohepatitis and metabolic disorders.[32] Dickkopf-3[33] and TNF receptor–associated factor 1[34] have also been shown to regulate ASK1 signaling and influence NAFLD progression. The deubiquitinating enzyme TNF-α-induced protein 1 suppresses polyubiquitination-dependent hyperactivation of ASK1 to ameliorate NASH.[35] Compared to these regulators, Dusp9 belongs to the MAPK phosphatase (MKP) family. MAPK hyperactivation in turn activates the MKPs to oppose their action, which forms a feedback regulation loop.[23] Thus, targeting Dusp9–ASK1 signaling, a physiological regulation loop, may provide an effective and reliable strategy for NASH treatment.

Collectively, the data presented here suggest that Dusp9 expressed by hepatocytes plays a pathologically important role in the development and progression of obesity, IR, hepatic steatosis, and regulation of inflammation, which largely depend on regulation of the ASK1–p38/JNK signaling axis. These findings suggest that specifically targeting hepatocyte Dusp9 may be a promising approach for treating hepatic steatosis and related metabolic dysfunctions.

REFERENCES

1) Clark JM, Diehl AM. Nonalcoholic fatty liver disease: an underrecognized cause of cryptogenic cirrhosis. JAMA 2003;289:3000-3004.
2) Spengler EK, Loomba R. Recommendations for diagnosis, referral for liver biopsy, and treatment of nonalcoholic fatty liver disease and nonalcoholic steatohepatitis. Mayo Clin Proc 2015;90:1233-1246.
3) **Farooq A, Zhou MM.** Structure and regulation of MAPK phosphatases. Cell Signal 2004;16:769-779.
4) Emanuelli B, Eberle D, Suzuki R, Kahn CR. Overexpression of the dual-specificity phosphatase MKP-4/DUSP-9 protects against stress-induced insulin resistance. Proc Natl Acad Sci USA 2008;105:3545-3550.
5) Patterson KI, Brummer T, O'Brien PM, Daly RJ. Dual-specificity phosphatases: critical regulators with diverse cellular targets. Biochem J 2009;418:475-489.
6) Pearson G, Robinson F, Beers Gibson T, Xu BE, Karandikar M, Berman K, et al. Mitogen-activated protein (MAP) kinase pathways: regulation and physiological functions. Endocr Rev 2001;22:153-183.
7) Camps M, Nichols A, Arkinstall S. Dual specificity phosphatases: a gene family for control of MAP kinase function. FASEB J. 2000;14:6-16.
8) Marie-Claire C, Benturquia N, Lundqvist A, Courtin C, Noble F. Characteristics of dual specificity phosphatases mRNA regulation by 3,4-methylenedioxymethamphetamine acute treatment in mice striatum. Brain Res 2008;1239:42-48.
9) Michelotti GA, Machado MV, Diehl AM. NAFLD, NASH and liver cancer. Nat Rev Gastroenterol Hepatol 2013;10:656-665.
10) Xu H, Dembski M, Yang Q, Yang D, Moriarty A, Tayber O, et al. Dual specificity mitogen-activated protein (MAP) kinase phosphatase-4 plays a potential role in insulin resistance. J Biol Chem 2003;278:30187-30192.
11) Brunt EM, Kleiner DE, Wilson LA, Belt P, Neuschwander-Tetri BA, NASH Clinical Research Network. Nonalcoholic fatty liver

disease (NAFLD) activity score and the histopathologic diagnosis in NAFLD: distinct clinicopathologic meanings. Hepatology 2011;53:810-820.
12) Wang XS, Diener K, Jannuzzi D, Trollinger D, Tan TH, Lichenstein H, et al. Molecular cloning and characterization of a novel protein kinase with a catalytic domain homologous to mitogen-activated protein kinase kinase kinase. J Biol Chem 1996;271:31607-31611.
13) Park JY, Kim Y, Im JA, Lee H. Oligonol suppresses lipid accumulation and improves insulin resistance in a palmitate-induced in HepG2 hepatocytes as a cellular steatosis model. BMC Complement Altern Med 2015;15:185.
14) Cai D, Yuan M, Frantz DF, Melendez PA, Hansen L, Lee J, et al. Local and systemic insulin resistance resulting from hepatic activation of IKK-beta and NF-kappaB. Nat Med 2005;11:183–190.
15) **Gehart H, Kumpf S,** Ittner A, Ricci R. MAPK signalling in cellular metabolism: stress or wellness? EMBO Rep 2010;11:834-840.
16) **Lin D, Li L,** Sun Y, Wang W, Wang X, Ye Y, et al. Interleukin-17 regulates the expressions of RANKL and OPG in human periodontal ligament cells via TRAF6/TBK1-JNK/NF-kappaB pathways. Immunology 2015;144:472-485.
17) Ray A, Sehgal N, Karunakaran S, Rangarajan G, Ravindranath V. MPTP activates ASK1–p38 MAPK signaling pathway through TNF-dependent Trx1 oxidation in parkinsonism mouse model. Free Radic Biol Med 2015;87:312-325.
18) Neuschwander-Tetri BA, Loomba R, Sanyal AJ, Lavine JE, Van Natta ML, Abdelmalek MF, et al. Farnesoid X nuclear receptor ligand obeticholic acid for non-cirrhotic, non-alcoholic steatohepatitis (FLINT): a multicentre, randomised, placebo-controlled trial. Lancet 2015;385:956-965.
19) Chalasani N, Younossi Z, Lavine JE, Diehl AM, Brunt EM, Cusi K, et al. The diagnosis and management of non-alcoholic fatty liver disease: practice guideline by the American Association for the Study of Liver Diseases, American College of Gastroenterology, and the American Gastroenterological Association. Hepatology 2012;55:2005-2023.
20) Arab JP, Arrese M, Trauner M. Recent insights into the pathogenesis of nonalcoholic fatty liver disease. Annu Rev Pathol 2018;13:321-350.
21) Tilg H, Moschen AR. Insulin resistance, inflammation, and non-alcoholic fatty liver disease. Trends Endocrinol Metab 2008;19:371-379.
22) **Glass CK, Olefsky JM.** Inflammation and lipid signaling in the etiology of insulin resistance. Cell Metab 2012;15:635-645.
23) Lawan A, Bennett AM. Mitogen-activated protein kinase regulation in hepatic metabolism. Trends Endocrinol Metab 2017;28:868-878.
24) Vernia S, Cavanagh-Kyros J, Garcia-Haro L, Sabio G, Barrett T, Jung DY, et al. The PPARalpha–FGF21 hormone axis contributes to metabolic regulation by the hepatic JNK signaling pathway. Cell Metab 2014;20:512-525.
25) Aguirre V, Werner ED, Giraud J, Lee YH, Shoelson SE, White MF. Phosphorylation of Ser307 in insulin receptor substrate-1 blocks interactions with the insulin receptor and inhibits insulin action. J Biol Chem 2002;277:1531–1537.
26) Kodama Y, Brenner DA. c-Jun N-terminal kinase signaling in the pathogenesis of nonalcoholic fatty liver disease: multiple roles in multiple steps. Hepatology 2009;49:6-8.
27) **Sumara G, Formentini I,** Collins S, Sumara I, Windak R, Bodenmiller B, et al. Regulation of PKD by the MAPK p38delta in insulin secretion and glucose homeostasis. Cell 2009;136:235–248.
28) Cao W, Collins QF, Becker TC, Robidoux J, Lupo EG Jr, Xiong Y, et al. p38 mitogen-activated protein kinase plays a stimulatory role in hepatic gluconeogenesis. J Biol Chem 2005;280:42731-42737.
29) Sookoian S, Pirola CJNAFLD. Metabolic make-up of NASH: from fat and sugar to amino acids. Nat Rev Gastroenterol Hepatol 2014;11:205-207.
30) **Saltiel AR, Kahn CR.** Insulin signalling and the regulation of glucose and lipid metabolism. Nature 2001;414:799-806.
31) Loomba R, Lawitz E, Mantry PS, Jayakumar S, Caldwell SH, Arnold H, et al. The ASK1 inhibitor selonsertib in patients with nonalcoholic steatohepatitis: a randomized, phase 2 trial. Hepatology 2018;67:549-559.
32) **Wang PX, Ji YX, Zhang XJ,** Zhao LP, Yan ZZ, Zhang P, et al. Targeting CASP8 and FADD-like apoptosis regulator ameliorates nonalcoholic steatohepatitis in mice and nonhuman primates. Nat Med 2017;23:439-449.
33) **Xie L, Wang PX, Zhang P,** Zhang XJ, Zhao GN, Wang A, et al. DKK3 expression in hepatocytes defines susceptibility to liver steatosis and obesity. J Hepatol 2016;65:113-124.
34) **Xiang M, Wang PX, Wang AB,** Zhang XJ, Zhang Y, Zhang P, et al. Targeting hepatic TRAF1–ASK1 signaling to improve inflammation, insulin resistance, and hepatic steatosis. J Hepatol 2016;64:1365-1377.
35) **Zhang P, Wang P-X, Zhao L-P,** Zhang X, Ji Y-X, Zhang X-J, et al. The deubiquitinating enzyme TNFAIP3 mediates inactivation of hepatic ASK1 and ameliorates nonalcoholic steatohepatitis. Nat Med 2017;24:84-94.

Author names in bold designate shared co-first authorship.

Supporting Information

Additional Supporting Information may be found at onlinelibrary.wiley.com/doi/10.1002/hep.30198/suppinfo.